ASEN 2004 Glider Lab: Computational Tool Development

Ryan Block*, Zach Lesan†, Cole MacPherson‡, Scott Mansfield§, and Ankrit Uprety¶
University of Colorado at Boulder, Boulder, Colorado, 80303

I. Results

A. Lift Curve Comparison

Figure 1 displays the relationship between the Whole Aircraft Coefficient of Lift, C_L, and the angle of attack of the wing, α. C_L was calculated by finding a_0 from the 2-d airfoil curve. a_0 was then used in Eq. (2) to find a. Eq. (3) was then utilized to find C_L. The lift curve slope, $\frac{dC_L}{d_\alpha}$, is the greatest for the provided 2-D airfoil data for the MH 32 airfoil and smallest for CFD Data and out estimated total body C_L.

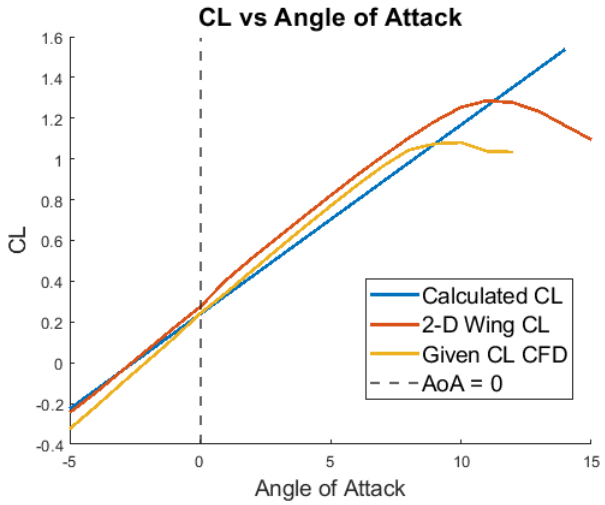

Fig. 1 CL vs. AoA

Intuitively, this makes sense because the values of C_L for each angle of attack should be greater for the 2D airfoil than for the 3D wings. In order to create lift, the pressure on top of the wing must be lower than the pressure below the wing. In three dimensions, the high pressure air below the wing is able to move into the lower pressure area above the wing by way of motion around around the wing tip. This is not possible on an "infinite" wing, which has no wing tips. This down-wash of air onto the top surface of the wing decreases the difference in pressure between the top and bottom surfaces of the wing, resulting in less lift generated. This can be seen in Fig. 1 by the decrease in C_L at each angle of attack except for the angle of attack corresponding to zero lift. Here, the difference in pressure between the top and bottom surface is zero, so there is no down-wash, and very little difference in the values of C_L provided by the various different methods.

Additionally, our calculated $\frac{dC_L}{d_\alpha}$ is not as accurate near the edges of the plot. This is due to our calculation of $\frac{dC_L}{d_\alpha}$ as a constant average of the linear portion of the plot, rather than a changing value throughout various angles of attack. Bearing in mind this discrepancy, our model of $\frac{dC_L}{d_\alpha}$ follows quite closely with the given CFD Data near the center of the plot, as to be expected.

*SID: 109210321
†SID: 108625270
‡SID: 108521239
§SID: 109029607
¶SID: 109025686

B. Drag polar comparison

Figure 3 displays the estimated C_D vs C_L plots, with calculations based on the estimated 3-D finite wing drag polar, whole aircraft drag polar and the drag polar from the CFD data. C_D was calculated using Eq. (4). e_0 and C_{D0} were calculated by setting up Eq. (7) and Eq. (11) as a system of equations (handwritten derivation in appendix). The wetted area was found by modeling the plane using CAD design in Solidworks. After modeling, the measure function gave an accurate estimate of the wetted area.

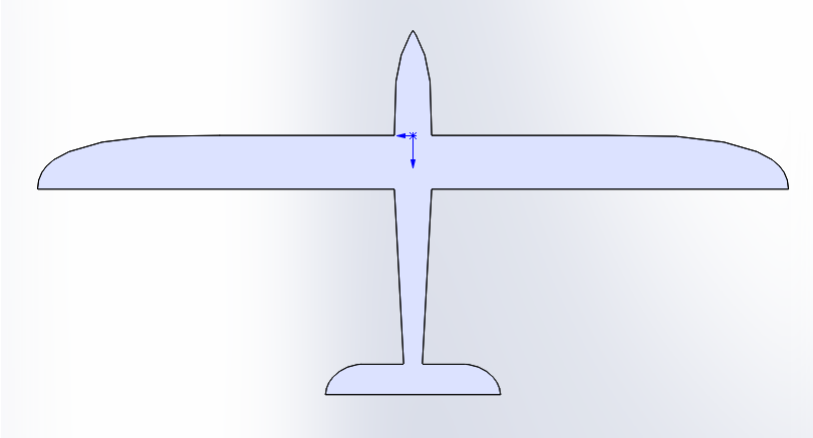

Fig. 2 Solidworks Glider CAD

The minimum percent error between the CFD data drag polar and our calculated whole aircraft drag polar is 20.7%, which occurs at C_{Dmin}, and the maximum is 65.8%, which occurs at the far right edge of the graph. The percent error increases in both directions as one moves away from the location of C_{Dmin}. The value of C_{Dmin} is entirely dependent on drag that is not due to lift, since it occurs at the angle of attack that corresponds to zero lift.

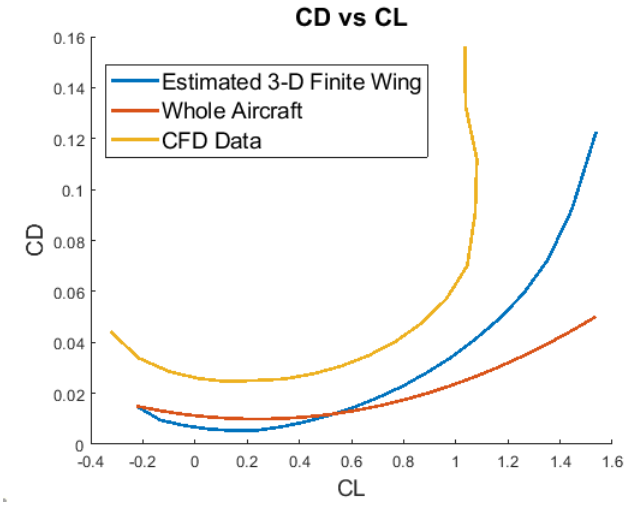

Fig. 3 Drag Polar

The further one gets from this point of C_{Dmin}, the more that drag-due-to-lift impacts the calculation of C_D. The behavior of the percent differences, which are lowest at C_{Dmin} and highest at the edge of the plot, indicate that there is greater error within the calculation of the drag-due-to-lift component of the total drag as opposed to the parasite drag, which is independent of the amount of lift.

The larger discrepancy in drag-due-to-lift components can be explained by our calculation of $\frac{dC_L}{d_\alpha}$, discussed in the previous section, which assumes a constant slope in the C_L vs Angle of Attack plot. This constant slope was calculated by averaging the varying slope values in the linear region of the 2D airfoil C_L vs α plot, and then converting this single

averaged value of a_0 into a. This resulted in a slope that is smaller than the given CFD data for the C_L vs Angle of Attack plot, so our calculated C_L is smaller than the given CFD C_L for a majority of the angles of attack. Since our drag-due-to-lift term is dependent upon C_L^2 and our calculated C_L is lower than the given CFD C_L, the edges of our calculated drag polar are lower than the given CFD drag polar and contain correspondingly increasing percent differences.

C. L/D Comparison

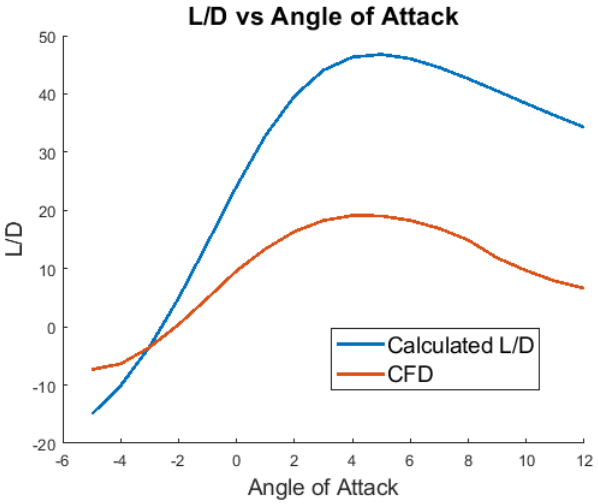

Fig. 4 L/D vs AoA

Figure 4 displays the estimated L/D along with the L/D of the CFD data. As shown from this graph, our maximum L/D value is 46 and it occurs at an angle of attack of five degrees. The velocity associated with these values is 16.03 m/s. Both the velocity and the angle of attack are similar to the CFD data but we largely stray away from the data when evaluating the L/D value. The velocity value using the CFD data was 15.7 m/s and the angle of attack was four degrees, both similar to values found with our calculations.

Our L/D values are significantly larger than those of the CFD data. it is worth noting that the general shape and trend of the curves are similar, so this large disparity could be attributed to error within the drag value calculations. The coefficient of drag values could not be found such that their values would match up with those of the CFD data. The percent difference in the calculated values and given CFD values for L/D begins at 51.2%, increases to near 60% near the maximum L/D values for either plot, and continues to increase to 80.7% at the right end of the plot. The percent error increases as angle of attack increases, which also corresponds to an increasing C_L for the all angles of attack between -5°and 12°.

This increase in percent difference as C_L increases can be attributed, once again, to the derivation of the slope of the C_L vs Angle of Attack graph, $\frac{dC_L}{d\alpha}$. Our estimated slope was lower than the CFD data, so the discrepancy between our C_L values and the CFD ones grows as C_L increases. The numerator and denominator of L/D, or the equivalent $\frac{C_L}{C_D}$, both depend upon C_L. However, the denominator C_D depends upon C_L^2, as shown in Equation (4), so it will grow faster than the numerator. Therefore, since our C_L values are smaller than the CFD values, our calculated L/D will be larger than the CFD values and continue to get larger by a greater and greater margin as angle of attack and C_L increase. This is displayed in both our calculated percent differences and Figure 4. While these percent differences may significantly impact the accuracy of our calculated L/D values compared to the CFD values, the location of our L/D max is still in roughly the same location as the CFD L/D max, resulting in a calculated velocity that is quite close to the velocity calculated based on the CFD values. It is thought that the error resides within the C_{LminD} or the C_{Dmin} calculations but after much investigation, an error could not be found.

D. Performance flight condition comparison

Glide Range and Endurance		
	CFD Values	Calculated Values
Velocity Req for Max Glide Range	15.7 m/s	16.03 m/s
Angle of Attack Req for Max Glide Range	4 °	5 °
Velocity Req for Max Glide Endurance	12.18 m/s	13.75 m/s
Angle of Attack Req for Max Endurance	6 °	10 °

The table above shows the flight conditions required to achieve both maximum range and maximum endurance, starting at a standard altitude of 1.8 km. Maximum range occurs when L/D is at a maximum. The C_L value at this point is used to find the velocity that the Tempest is required to fly at to achieve maximum range. The percent difference in velocity between the given data and the calculated value is 2.12% . The percent difference for angle of attack is 25%. The small difference in the angles of attack can be explained by Fig. (4). Although the magnitude of each L/D is very different, their maximums both occur at very similar angles of attack. Figure (3) shows that the maximum $\frac{C_L}{C_D}$ for both the CFD data and calculated values are very similar. Equation (1) shows that this leads to very similar velocities because all other variables are the same for both sets of data.

Maximum endurance occurs when the power required is at a minimum. This is where $\frac{(C_L)^{\frac{3}{2}}}{C_D}$ is at a maximum. By finding the C_L at this maximum value, the velocity was once again found using Eq. (1) for both the given data and the calculated values. The percent difference for the velocity between the given data and the calculated value is 11.4%. The percent difference for the angle of attack between the given data and the calculated value is 40 percent. This large percent difference in angle of attack can be explained by Fig. (4). The $\frac{L}{D}$ curve for the CFD data has different curvature from the calculated $\frac{L}{D}$ curve. This means that the maximum value of $\frac{(C_L)^{\frac{3}{2}}}{C_D}$ occurs at different angles of attack for each set. The C_L values also slightly differ, which explains the slight difference in velocities.

E. Modifications to analytical tools for analyzing small UAS

One aspect of the computational tool that would benefit from change is the approximation used for C_{fe}, which is currently the average between the C_{fe} for a dirtier propeller aircraft, 0.0055, and the C_{fe} of a clean glider aircraft, 0.003. Since our designed glider will have no powered components, and thus no propeller, then the lower C_{fe} value of 0.003 is a much better assumption for our model. This is effectively a way to account for the reduction in induced drag from configuration when changing a design from a full UAV to a simple glider.

Further, it was determined that a factor of 2, multiplied by the C_D, made the calculated $\frac{L}{D}$ align much closer with the $\frac{L}{D}$ provided, however, without sufficient aerodynamic evidence to reinforce the scaling factor, we could not reasonably apply it to our code. One area of further interest would be to look into the discrepancies in C_D values and the validity of the scaling factor, and to find a justification to apply said factor to further labs. It is important to reiterate the fact that this scaling factor, while observed, is not utilized in any capacity in the final version of the code and plots.

An additional area of possible improvement is the calculation of Oswald's Efficiency Factor, which we did in this lab with Eq. (7) and Eq. (11) as a system of equations (handwritten derivation in appendix). However, a differently proportioned aircraft, which our future glider may well be, could constitute a different relationship between e_0 and C_{Do} than Eq. (7). This change in C_{Do} would affect our calculations of all drag not due to lift, which would better align the minimum value of our drag polar with the minimum value of the CFD drag polar and better align the maximum calculated L/D value with the maximum CFD L/D value. In order to better estimate the areas of the L/D plots and drag polar that are not constrained to drag, we could estimate the slope of the C_L vs angle of attack plot in more rigorous manner, specifically by not averaging the values and taking into account smaller variations within the linear portion of the plot.

While the computational tool developed lacks accuracy in C_D and $\frac{L}{D}$, the model still has value in the finite wing calculations and in the overall trends of the data. With the change to the C_{fe} and a greater level of scrutiny applied to future results, the computational tool can be shown to be very useful. Without further aerodynamic principles guiding modifications to the code, the inaccuracy of the models used must be accepted at this time.

References

[1] Anderson, J. D., Introduction to Flight, 8th Ed., McGraw Hill (2012).

[2] Brandt, S, Introduction to Aeronautics: A Design Perspective, 2nd Ed, AIAA (2004).

[3] Drela, M., XFOIL Program, MIT, https://web.mit.edu/drela/Public/web/xfoil/

[4] Kroo, I., Aircraft Design: Synthesis and Analysis, Stanford University, AA241, 2012.

[5] Nita, M., Scholz, D., Estimating the Oswald Factor from Basic Aircraft Geometrical Parameters, Hamburg University of Applied Sciences, 2012.

[6] Raymer, D. P., Aircraft Design: A Conceptual Approach, 2nd Ed., AIAA Inc., Chap. 12 (2012).

[7] Roskam, J., Airplane Design Part II: Preliminary Configuration Design and Integration of the Propulsion System, Chapter 12, DARCorporation (1997).

[8] Roskam, J., Airplane Design Part VI: Preliminary Calculation of Aerodynamic, Thrust, and Power Characteristics, Chapter 5, DARCorporation (1997).

[9] Roadman, J., Elston, J., Argrow, B., and Frew, E., "Mission Performance of the Tempest Unmanned Aircraft System in Supercell Storms," Journal of Aircraft, Vol. 49, No. 6, pp. 18211830 (2012).

[10] Selig, M., University of Illinois at Urbana-Champaign Applied Aerodynamics Group, https://mselig.ae.illinois.edu/index.html

Appendix

$$C_L = \frac{W}{\frac{1}{2}\rho V^2 S} \tag{1}$$

$$a = \frac{a_o}{1 + \frac{57.3 * a_o}{\pi * e * AR}} \tag{2}$$

$$C_L = a * (\alpha - \alpha_{L=0}) \tag{3}$$

$$C_D = C_{Do} + k_1 * C_L^2 + k_2 * C_L \tag{4}$$

$$k_1 = \frac{1}{\pi * e_o * AR} \tag{5}$$

$$k_2 = -2 * k_1 * C_{LminD} \tag{6}$$

$$e_0 = \frac{1}{\frac{1}{0.99 * s} + 0.38 * C_{Do} * \pi * AR} \tag{7}$$

$$s = 1 - 2 * (\frac{d_{fuselage}}{b})^2 \tag{8}$$

$$C_{Do} = k_1 * C_L^2 \tag{9}$$

$$3 * C_{Do} = k_1 * C_l^2 \tag{10}$$

$$C_{Do} = C_{Dmin} + k_1 * C_{LminD}^2 \tag{11}$$

$$C_{Dmin} = C_{fe} * \frac{S_{wet}}{S_{ref}} \tag{12}$$

$$e_0 = \frac{1}{\frac{1}{0.99s} + 0.38 C_{D_0} \pi AR}$$

$$C_{D_0} = C_D + k_1 C_L^2 \quad , \quad k_1 = \frac{1}{\pi e_0 AR}$$

$$C_{D_0} = C_D + \frac{1}{\pi e_0 AR} C_L^2$$

$$C_{D_0} = C_D + \frac{1}{\pi \left(\frac{1}{\frac{1}{0.99s} + 0.38 C_{D_0} \pi AR} \right) AR} C_L^2$$

$$C_{D_0} = C_D + \frac{C_L^2}{\pi AR \left(\frac{1}{0.99s} + 0.38 C_{D_0} \pi AR \right)}$$

$$C_{D_0} = C_D + \frac{C_L^2}{1} \cdot \frac{\frac{1}{0.99s} + 0.38 C_{D_0} \pi AR}{\pi AR}$$

$$C_{D_0} = C_D + \frac{\frac{C_L^2}{0.99s} + 0.38 C_{D_0} \pi AR C_L^2}{\pi AR}$$

$$C_{D_0} \pi AR = C_D \pi AR + C_L^2 \left(\frac{1}{0.99s} + 0.38 C_{D_0} \pi AR \right) - 0.38 C_{D_0} \pi AR C_L^2$$

$$C_{D_0} \pi AR - 0.38 C_{D_0} \pi AR C_L^2 = C_D \pi AR + C_L^2 \frac{1}{0.99s}$$

$$C_{D_0} \left(\pi AR - 0.38 \pi AR C_L^2 \right) = C_D \pi AR + C_L^2 \frac{1}{0.99s}$$

$$C_{D_0} = \frac{C_D \pi AR + C_L^2 \frac{1}{0.99s}}{\pi AR - 0.38 \pi AR C_L^2}$$